Full Electrothermal OLED Model Including Nonlinear Self-heating Effects

Axel Fischer,[1,*] Manuel Pfalz,[1] Koen Vandewal,[1] Simone Lenk,[1] Matthias Liero,[2] Annegret Glitzky,[2] and Sebastian Reineke[1]

[1]*Dresden Integrated Center for Applied Physics and Photonic Materials and Institute for Applied Physics, Technische Universität Dresden, Nöthnitzer Straße 61, 01187 Dresden, Germany*

[2]*Weierstrass Institute for Applied Analysis and Stochastics, Mohrenstraße 39, 10117 Berlin, Germany*

Organic light-emitting diodes (OLEDs) are widely studied semiconductor devices for which a simple description by a diode equation typically fails. In particular, a full description of the current-voltage relation, including temperature effects, has to take the low electrical conductivity of organic semiconductors into account. Here, we present a temperature-dependent resistive network, incorporating recombination as well as electron and hole conduction to describe the current-voltage characteristics of an OLED over the entire operation range. The approach also reproduces the measured nonlinear electrothermal feedback upon Joule self-heating in a self-consistent way. Our model further enables us to learn more about internal voltage losses caused by the charge transport from the contacts to the emission layer which is characterized by a strong temperature-activated electrical conductivity, finally determining the strength of the electrothermal feedback. In general, our results provide a comprehensive picture to understand the electrothermal operation of an OLED which will be essential to ensure and predict especially long-term stability and reliability in superbright OLED applications.

I. INTRODUCTION

Organic light-emitting diodes (OLEDs) have become the standard technology for smartphone displays and will also take the lead in the TV market soon [1,2]. New applications requiring considerably higher brightnesses than displays (>100 cd/m^2) or lighting (>1000 cd/m^2) are envisioned. In particular, signaling in the automobile sector is attractive, as new design possibilities allow clearly visible elements to be incorporated, helping to make cars more distinguishable and appealing. However, the use of OLEDs as tail lights, turn lights, or even break lights involves super-bright operation ($>10\,000$ cd/m^2) in order to fulfill international regulations. OLEDs are highly attractive as desired red-orange devices have become very efficient. The required level of luminance is achieved and at the same time they are much more stable than, for example, blue OLEDs since red OLEDs do not suffer from high triplet energies [3].

Another issue accompanying high brightness is the strongly enhanced power dissipation, leading to Joule self-heating [4,5]. Apart from a possible degradation of the OLED due to warming, self-heating has the negative effect that the lateral brightness becomes very inhomogeneous, canceling out the benefits of the OLED technology being a truly scalable area light source [6]. Furthermore, OLEDs tend to show a very strong electrothermal feedback, which involves a positive feedback loop between current flow, power dissipation, and temperature increase [7]. This behavior is due to the widely observed temperature-activated conductivity in organic semiconductor devices which is also the case for OLEDs [8–10]. If self-heating comes into play, the steady increase of the current flow and the power dissipation, when driven at a constant voltage, can even lead to an abrupt destruction of a device by thermal runaway [11]. The use of a constant current operation, or a series resistor, can prevent the underlying thermal-switching process, but not the fact that OLED emission becomes inhomogeneous at high injection currents. Besides that, strong electrothermal feedback eventually leads to a current-voltage regime of S-shaped negative differential resistance (S NDR) [7,11], which increases the complexity of predicting the device's behavior [12].

Another difficulty OLED technology faces for superbright applications, besides internal Joule heating, is the external variation of the ambient temperature, which can change the driving current and the light output as well. Thus, an accurate and reliable model to understand the current-voltage-temperature relation of an OLED is essential for further progress in this field.

Here, we will introduce a physics-motivated explicit description of OLED current-voltage curves at various

---

*Corresponding author: axel.fischer@iapp.de; www.iapp.de

014023-1

temperatures. The model is validated with experimental data and is used to predict the electrothermal feedback by incorporating a global equation for the heat conduction. Moreover, our approach integrates a full temperature-dependent description of the recombination-related current flow, which enables us to quantify internal voltage losses. Analyzing the contribution of different parts of the OLED to the overall device resistance further reveals where the activation of the electrical conductivity originates from.

II. RESULTS

In our work, we prepare small molecule organic devices by thermal vapor deposition on precleaned glass substrates. Two perpendicular oriented electrodes sandwich the layer stack and realize a sample with crossbar geometry. The current-voltage curves are measured by four-wire measurements as shown in Ref. [7]. Each of the electrodes can be contacted from two sides: on the one hand, to supply the device with current, and on the other hand, to measure the potential which is present at the device. This technique allows us to remove the effect of series resistance of the electrodes outside the active area to the measurement, which is especially important if very high current densities are measured and the resistance of the device becomes close to external resistances. For example, the temperature-activated electrical conductivity of the devices could otherwise be strongly affected by series resistance at the highest temperatures and voltages. The active area of the OLEDs is 6.5 mm^2, whereas the active area of single-carrier devices has been varied (see Fig. S1 in the Supplemental Material [13]) to reach high current densities without significant self-heating [14].

All investigations are based on a red OLED stack using a p-doped–intrinsic–n-doped (p-i-n) layer sequence [cf. Fig. 2(b)] with a 20-nm-thick emission layer comprising the emitter Ir(MDQ)$_2$(acac) at 4 wt % in a Spiro-TAD matrix. The used materials are widely known in the literature [15,16] and are chosen to achieve a temperature-stable layer stack. The OLED layer stack and the definition of all materials are given in the Supplemental Material [13]. Electrodes are prepared to aim for light emission through the top electrode. This assembly has the benefit that the samples can be cooled by a Peltier element in thermal contact with the glass substrate at the bottom, without blocking the light outcoupled to the top [see Fig. 2(b)]. The temperature variation is performed in a vacuum cryostat and a Keithley 2602A measures all current-voltage characteristics using the measurement software SweepMe! [17]. All devices are encapsulated with an epoxy glued glass, and a detailed description of the substrate and the encapsulation geometry can be found in Ref. [18].

Figure 1 shows current-voltage characteristics, displaying the effects of self-heating. A measurement with a
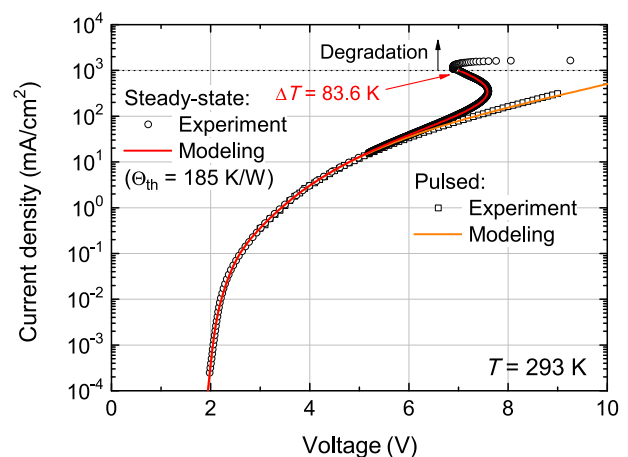

FIG. 1.   Experimental current-voltage curve of an OLED in steady state shows a regime of negative differential resistance after the voltage turnover (7.6 V) takes place at a current density of about 360 mA/cm^2. Our electrothermal model takes this into account by allowing for a positive feedback between the temperature, the voltage-dependent characteristic $j = j(V, T)$, and the power-dependent temperature increase. For comparison, a pulsed measurement shows no electrothermal feedback but fully agrees with the steady-state curve in the range from 1 to 10 mA/cm^2. Reducing the thermal resistance to 0 K/W, the modeled curve also agrees with the pulsed measurement. The model allows determination of a maximum temperature increase of 83.6 K, yielding a temperature of 103.5 °C at the point shortly before abrupt degradation occurs, starting from about 1000 mA/cm^2.

pulsed voltage (open squares) of 200 μs and 1000 times longer off time reveals a typical current-voltage relation: The current rises with increasing voltage and the slope in this semilogarithmic plot decreases. However, we observe a different behavior when a steady-state measurement (open circles) with a dense number of points, each held for 1 s, is performed. For voltages higher than 6 V, the steady-state current-voltage curve deviates from the pulsed measurement, exhibiting a strong growth of the current with voltage. At about 7.6 V, the steady-state curve displays a voltage turnover, and now the voltage decreases with a further increase of applied current. Thereafter, the OLED enters an operation regime of S NDR. It is the aim of this work to explain this behavior by relating it to the temperature-activated electrical conductivity of the OLED.

In order to understand whether such S NDR behavior can be fully explained by its temperature-activated electrical conductivity, we have to obtain an explicit expression $j = j(V, T)$. This current-voltage-temperature relation is then used to model the electrothermal feedback. Our approach considers the following three important processes in OLED operation: hole conduction (p system), recombination, and electron conduction (n system).
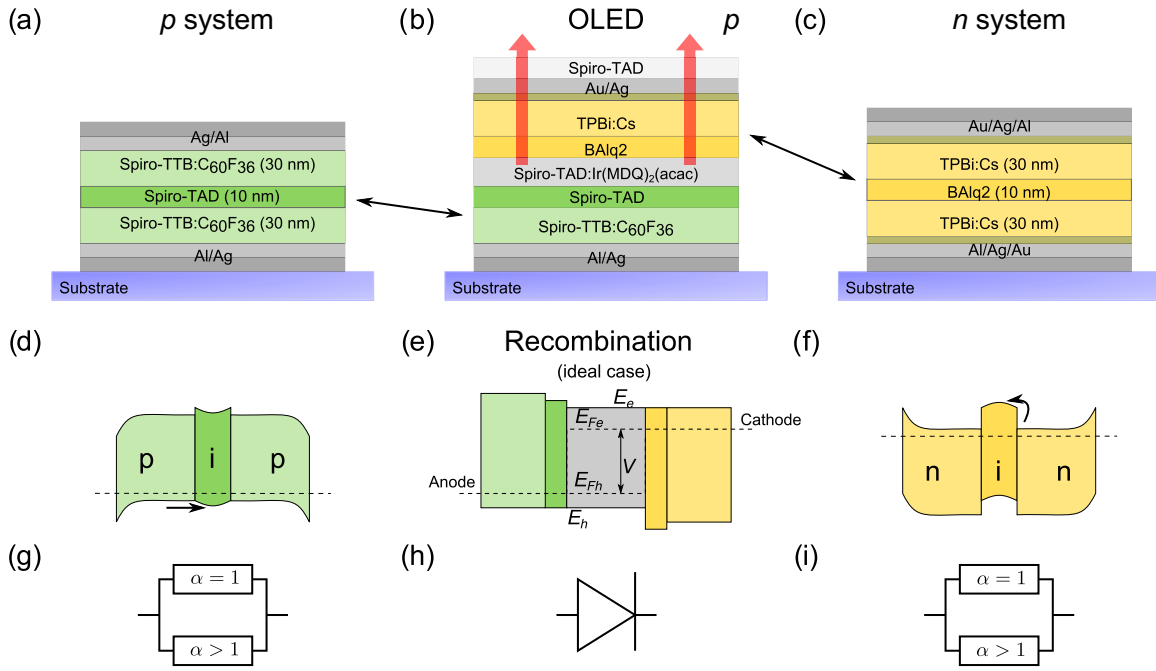
FIG. 2. Three different devices are investigated: devices of (a) p-doped–intrinsic–p-doped layers or (c) n-doped–intrinsic–n-doped layers mimic the hole transporting p system, and the electron transporting n system, respectively, as used in the full OLED stack, see (b). Simplified energy diagrams are shown in (d)–(f) corresponding to (a)–(c). (e) Recombination is simplified, described by assuming a homogeneous recombination within a certain region, e.g., the emission layer (EML, gray). The energetic distances and barriers of the energy diagram have no direct relation to the investigated experimental structure but simply represent the ideal case that the intrinsic charge blocking layers restrict recombination to the EML. In that case, the quasi-Fermi-levels for electrons E_{Fe} and for holes E_{Fh} are splitted by the applied voltage V. The conduction level for electrons E_e and the valence level for holes E_h are denoted as well. The OLED stack in (b) is modeled by connecting the elements in (g) p system, (h) recombination, and (i) n system in series.

The recombination current j_{rec} within the device is modeled by a simplified, homogeneous diode equation

$$j_{\mathrm{rec}}(V,T) = j_{00} \exp\left(\frac{eV - E_{a,0}}{n_{\mathrm{id}} k_B T}\right), \qquad (1)$$

assuming that recombination takes place between electrons and holes via two distinct states of an energetic distance $E_{a,0}$ and the quasi-Fermi-levels for electrons and holes describe their charge-carrier densities, assuming a Boltzmann distribution. As visualized in Fig. 2(e), the split of quasi-Fermi-levels is related to the applied voltage V. The ideality factor n_{id} considers nonideal recombination, typically being between 1 (e.g., bimolecular recombination) and 2 (e.g., trap-assisted recombination) [19]. The prefactor j_{00} is here a temperature- and voltage-independent constant, which describes the maximum possible recombination current density, if all states would permanently be filled and recombine with their related recombination time. Since we model experimental data at voltages above 1.5 V, we fully neglect thermal charge generation.

The activation energy of the related electrical conductivity in the voltage range dominated by recombination current is thus given by

$$E_a(V) = \frac{E_{a,0} - eV}{n_{\mathrm{id}}}. \qquad (2)$$

Here, $E_{a,0}/n_{\mathrm{id}}$ is the effective activation energy of the recombination (and generation) current at zero voltage.

To understand the limitations of the current flow, unrelated to recombination, we build devices consisting of p-doped–intrinsic–p-doped (p-i-p) layers or n-doped–intrinsic–n-doped (n-i-n) layers, shown in Figs. 2(a) and 2(c). The idea is that these devices include the same material combinations and thus the same charge injection, the same internal energy barriers, and the same intrinsic layer as used in the complete OLED stack. The p and the n systems are then both described by a combination of a linear ($\alpha = 1$) and a nonlinear ($\alpha > 1$) temperature-activated current-voltage law

$$j = j_{\mathrm{ref}} \left(\frac{V}{V_{\mathrm{ref}}}\right)^{\alpha} \exp\left[-\frac{E_a}{k_B}\left(\frac{1}{T} - \frac{1}{T_{\mathrm{ref}}}\right)\right] \qquad (3)$$

with T_{ref} and V_{ref} being arbitrarily chosen reference values that are set to 293 K and 1 V, respectively. The prefactor

j_{ref} is a current density for the above given reference conditions and tunes the conductivity range. The electrothermal feedback of this kind of parametrization is studied in detail in Ref. [11]. Figures 2(g) and 2(i) show the parallel connection of the linear and the nonlinear element, for the p and the n system, respectively.

These three parts, the p system, the recombination, and the n system are later put into a series connection in order to calculate the total voltage consumption of the OLED at a given current level. Thus, the final model represents the circuit elements visualized by Figs. 2(g)–2(i) in series.

A. Discussion of the fit

Fitting of the experimental data is performed manually and has to be understood as a global fit of different data sets (Figs. 1, 3, and 4). Figures 3 and 4 are measured at different temperatures and can be considered to be isothermal. First, the parameters for the recombination are adjusted according to Eq. (1) to match the exponential current-voltage regime in the voltage range from 1.5 to 2.0 V. Measurement points below 1.5 V are related to leakage current and are not considered. In a next step, the parameters for the p system and the n system are determined by fitting the data according to Eq. (3) to match the observed range of currents and voltages. The combined set of parameters is then used to compare with Fig. 4(a) and further adjusted with a priority on fitting the current-voltage characteristics of the complete OLED. The fits are weighted towards curves of room temperature and higher temperatures; it is most essential to later match the electrothermal feedback in Fig. 1, which also starts from room temperature. Here, attention is given to achieving almost perfect agreement with the measurement of the electrothermal feedback in Fig. 1. Table I lists this global parameter set describing all modeled data in this work. The result of the fitting procedure will now be discussed for the three different sets of experimental data.

TABLE I. Global constant parameter set to fit and model all experimental data in this work.

	Recombination	
j_{00}	40 A/cm^2	
$E_{a,0}$	2.72 eV	
n_{id}	1.55	
	p-system linear	*p*-system nonlinear
α	1.0	3.7
j_{ref}	1 mA/cm^2	8.1 mA/cm^2
E_a	0.275 eV	0.25 eV
	n-system linear	*n*-system nonlinear
α	1.0	3.07
j_{ref}	0.1 mA/cm^2	3.6 mA/cm^2
E_a	0.5 eV	0.325 eV

1. Fitting of the p and n systems

In order to investigate the losses due to potential drops outside the emission layer, we build single-carrier devices resembling either the electron-conducting or hole-conducting system of the OLED. They consist of a central 10-nm-thick intrinsic layer embedded between two 30-nm-doped layers, shown in Figs. 2(a) and 2(c). In that manner, they have the same charge injection, the same energy barriers between the doped layer and the intrinsic layer, and the same charge transport through the intrinsic layer as it occurs in the complete OLED.

The measured current-voltage characteristics for different temperatures are presented in Figs. 3(a) and 3(b). A general observation is that curves of these kinds of devices are linear at low voltages, i.e., voltages below about 300 mV, but become superlinear at higher voltages. At low voltages, a residual background conductivity typically leads to the fact that the current is proportional to the applied voltage and at higher voltages, space-charge-limited currents (SCLCs) lead to a steeper increase of the current-voltage characteristics [20–23]. In order to model this behavior, a simple resistive network is used, based on two parallel resistors: a linear and a nonlinear one, as drawn in Figs. 2(g) and 2(i). Basically, these resistors follow a power law according to Eq. (3), where the exponent α is either 1 (linear) or >1 (nonlinear). To account for the temperature dependence, both resistors have a temperature-activated conductivity with an individual activation energy E_a, see Eq. (3). The use of such an Arrhenius-like law to describe the activation of charge-transport phenomena in organic semiconductors has often been discussed in the literature. This behavior can be related to charge-hopping transport, overcoming injection barriers as well as internal energy barriers [8,24–27].

This simplified phenomenological approach does not allow the experimental data to be covered exactly. Still, it has several advantages: It reproduces the qualitative behavior of the single-carrier devices, i.e., the change from a linear to a nonlinear current-voltage relation, it matches the right order of magnitude of the conductance for each system and can roughly reproduce the temperature dependence. Of course, one could add further nonlinear resistors in parallel to achieve an even better agreement. However, here we want to understand the basic influence of voltage losses of the p and n systems on the characteristics of the complete OLED and how both systems influence the electrothermal feedback.

The fit in Fig. 3 contains three parameters for each system: The current density j_{ref} scales the basic conductivity and is related to an arbitrarily chosen reference temperature and reference voltage, i.e., 293 K and 1 V, respectively. The exponent of the voltage dependence α adjusts the slope of the curves, and the activation energy E_a defines the temperature-dependent spread of the curves, according to the Arrhenius law used in Eq. (3).

We find that different activation energies have to be used, decreasing when changing from the linear to the nonlinear regime. Figures 3(c) and 3(d) show this in more detail by presenting the modeled effective activation energy of the electrical conductivity at each voltage. It becomes obvious that the activation energy is constant in the voltage range where either the linear or the nonlinear characteristic dominates, but has a more complex voltage dependence in the transition region, typically in the range of some 100 meV. The direct comparison between the p and the n system reveals that the conduction of electrons introduces the largest activation energy of up to 0.5 eV in the linear regime, changing to 0.325 eV in the nonlinear regime. In Fig. 3(b), it can be seen that the experimental curves are closer to each other for the highest voltages than predicted by the model. This reduced spread of the curves corresponds to a reduced activation energy, which is not captured by our approach.

The p system has activation energies lower than those of the n system in the entire voltage range. Again, the variation of the experimental curves is smaller at the highest voltages than predicted by the fit, which we ignore for sake of simplicity in order to keep the model approach simple. By comparing the corresponding currents in Table I, it can be seen that the p system generally has a higher conductivity compared to the n system by a factor of about 3–10.

Please note that these n-i-n and p-i-p devices resemble parts of the complete OLED but are not identical to them, which is why there is no need to aim for a perfect agreement by default. Still, these single-carrier devices allow the basic conductivity and the qualitative behavior of the current-voltage relation of each system to be adjusted as they contain essential parts of the OLED, such as the charge injection as well as the internal energy barrier between the doped and the intrinsic layer.

2. Recombination

The exact parameters found for the p and the n system are now also used to model the current-voltage relation of a complete OLED [see Fig. 2(b)]. In contrast to n-i-n or p-i-p devices, an OLED is a device consisting of a p-doped–intrinsic–n-doped layer stack. There, charges do not travel through the complete device but rather recombine with each other inside the device in the emission layer where ultimately light is generated. As a consequence, OLEDs have a diode character including an exponential current-voltage regime related to the exponentially increasing occupation of the molecular states. Whenever other potential drops, e.g., due to charge transport, are negligible, the related split of the quasi-Fermi-levels agrees with the externally applied voltage and an exponential relation can be seen in the experiment for the current-voltage curves, see Fig. 4(a) between 1.5 and 2.0 V.

Despite being well-known and heavily applied to inorganic LEDs, the relation between the current-voltage curve and the charge-carrier recombination is rarely addressed in the field of OLEDs [28]. There are only a few publications which deal with the extraction of parameters from the exponential current-voltage regime even though it is the most interesting regime to learn about recombination mechanisms in OLEDs [19,29]. In particular, less effort has been spent to extract the energy gap, at which free charge carriers start to recombine. The well-known Shockley equation describes ideal p-n junctions and has a temperature dependence which is therefore related to the diffusion
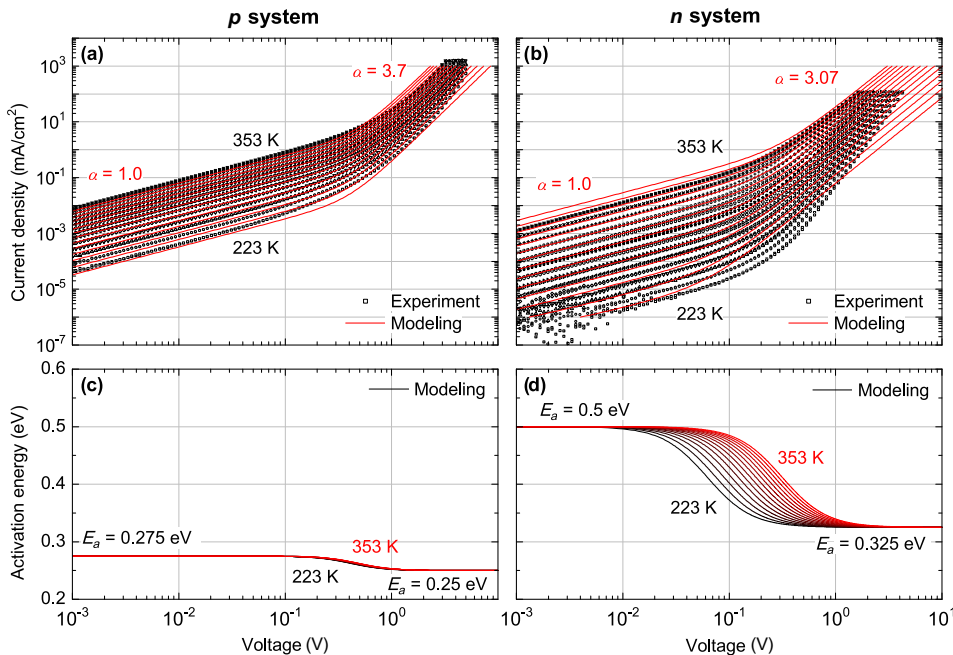

FIG. 3. Experimental current-voltage curves from 223 to 353 K superimposed with a fit by our global model for (a) the p system and (b) the n system. The activation energies resulting from the model are shown in (c) and (d), respectively. Generally, the activation energy decreases when the device operation goes from the linear to the nonlinear voltage range.
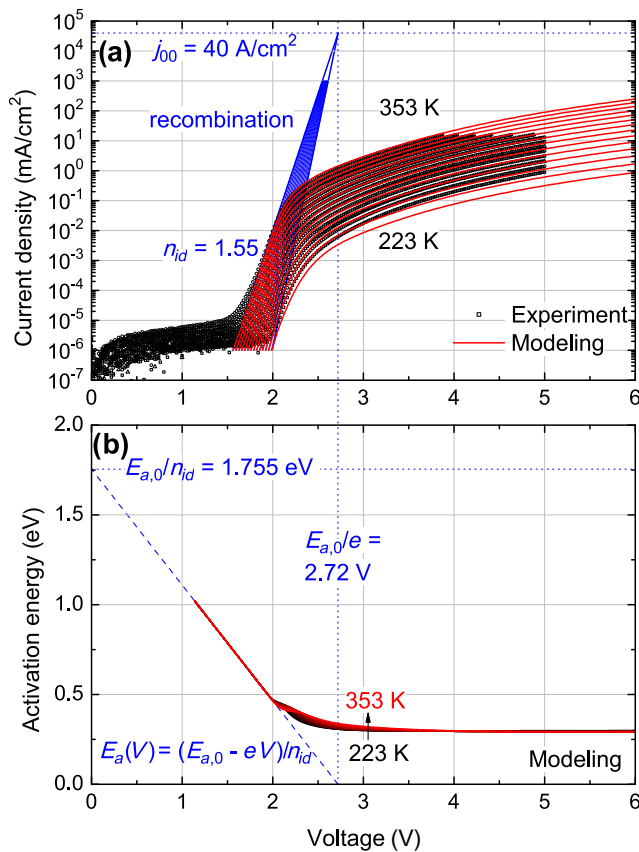
FIG. 4. (a) Fitting of the experimental current-voltage curves from 223 to 353 K by the model approach shown in Fig. 2. Leakage currents mainly below 1.5 V are not considered. Blue indicates recombination-related aspects. (b) Modeled activation energies resulting from the fit in (a) show a linear decrease at voltages below 2 V (recombination) and a saturation around 0.3 eV for larger voltages, related to the p and the n system of the OLED.

of charge carriers into the oppositely doped regions [30]. In the case of OLEDs, this approach is not suitable as there are additional intrinsic layers around the central emission layer reducing the charge-carrier diffusion. To start with a first analysis, we use the diode equation of Eq. (1) assuming homogeneous recombination in a certain region, e.g., the emission layer [see Fig. 2(h)]. As a result, a simplified temperature dependence related to the energy gap $E_{a,0}$ between the two states over which recombination takes place and the applied voltage V is achieved. The effective activation energy of the electrical conductivity at each voltage is then simply related to the difference of $E_{a,0}$ and eV [see Eq. (2)]. Such an approach is used in the field of organic solar cells and simple polymer LEDs to investigate recombination, but has not been transferred to state-of-the-art OLEDs consisting of several small molecule layers [31–33]. One reason is that parasitic losses are much more

pronounced in OLEDs in contrast to conventional LEDs as there is a huge difference in charge-carrier mobility.

The system is only fully determined if the respective voltage and temperature dependence are simultaneously captured. Fitting of the recombination current [blue text and lines in Fig. 4(a)] is performed for the voltage range between 1.5 and 2.0 V and is supported by the fact that we know about the influence of the p and n systems as obtained above. Thus, we have to adjust a much steeper exponential behavior as one might expect if a drift limitation would not be incorporated to get an agreement between experiment and model. We find that for voltages above 2.0 V, the experimental data are already affected by parasitic losses arising from drift limitations outside the recombination region.

Next, the three parameters of the recombination obtained by the global fit is discussed. The ideality factor n_{id} is 1.55, a value between the classical cases being $n_{id} = 1$ for direct recombination and being $n_{id} = 2$ for a recombination via an intermediate state, e.g., as described by Shockley-Read-Hall recombination [19,34,35]. In this work, this value remains reasonable and is not discussed further. We additionally find that recombination takes place at an energy of $E_{a,0} = 2.72$ eV, which is about 0.8 eV larger than the average photon energy emitted by this OLED structure (see Fig. S2 in the Supplemental Material [13]). The most reasonable explanation is that there are intrinsic losses in OLEDs during the recombination. First, recombination can take place on matrix molecules which have a higher exciton energy than the emitter molecules. Furthermore, the formed excitons are particles which have a lower energy than the two participating free charge carriers due to Coulomb attraction and relaxation, which is even more distinct for triplet states. Finally, one also has to assume a relaxation to the ground state of the exciton itself on the matrix molecule as well as on the emitter molecule. All together, these losses between the energy of the free charge carriers before starting the recombination process and the energy of the emitted photons are much higher in comparison to inorganic LEDs where, due to the low binding energy of the excitons, the emitted light has an energy close to the energy gap [36]. Eventually, the fit of the recombination current allows for the extraction of $j_{00} = 40$ A/cm^2, which is the maximum current density that can flow if all states were permanently filled and recombined with their recombination time. The fitted value can easily shift up and down with slight changes of the steepness of the exponential regime and is therefore rather an estimation of the order of magnitude. In order to get a feeling for which maximum recombination current one can expect due to the decay of excited triplet states, we estimate j_{00} based on the $d_{EML} = 20$ nm thick emission layer doped with approximately $c = 10\%$ emitter molecules. The employed emitter Ir(MDQ)$_2$(acac) has a decay time of $\tau \sim 2$ μs and the density of states is taken

to be $N_{st} = 10^{21}$ cm^{-3} [37–39]. Using the equation

$$j_{\text{decay, max}} = \frac{c \, d_{\text{EML}} \, e \, N_{st}}{\tau}, \qquad (4)$$

it becomes obvious that the emitter molecules in our OLED are not able to support a recombination current of more than 16 A/cm^2, already of the same order of magnitude as the fitted value for j_{00}. Of course, this value will hardly be achieved in an experiment as annihilation or quenching of the triplet states will set in much earlier [40]. Still, the experimental data at very low current densities and thus very low excitations, where parasitic effects mentioned above are negligible, exhibit the full information about the recombination system. Thus, investigating OLEDs at very low brightness and very low currents is of particular interest when studying recombination and also learning about the operation at application relevant current densities.

Incorporating the recombination to our model not only leads to a full electrothermal model describing the temperature and voltage dependence over a large range of current densities, but also helps to understand the operation of OLEDs. For example, the voltage at which the brightness of an OLED reaches a certain level, described by the turn-on voltage, is fully determined by the occupation of the molecular states by free charge carriers and their recombination. This fact is often discussed ambiguously in the field of OLEDs. Furthermore, the built-in potential of an OLED has no meaning for the exponential regime and cannot be used to understand at which voltage the current flow starts to increase rapidly. The often used built-in voltage is thus more or less a helping construct to adjust the modeled or simulated data to the right voltage range. Our study also makes it clear that more attention has to be given to investigating recombination as there is still the open question, how j_{00}, $E_{a,0}$, and n_{id} can be understood in a general picture. It is still unclear how the composition of the emission layer, the thickness of the layers, the use of blocker materials, or the energy gap of the used material, as well as many other factors, influence the recombination current. However, such investigations have to be part of further studies and are not addressed here.

Interestingly, an energy barrier between the hole-blocking layer made by BAlq2 and the emission layer is interestingly not needed to explain the data although the LUMO energy values of Spiro-TAD and BAlq2 differ quite a lot by ca. 0.9 eV (see [16]). Due to that barrier, it is likely that charges do not enter the LUMO states of Spiro-TAD, but are rather transported via the LUMO states of the emitter molecules, consequently lowering the energy barrier for electrons to enter the emission layer. Furthermore, charge exchange between these layers as well as surface-charge sheets due to permanent dipoles of oriented molecules can lead to an interfacial energetic shift

[41,42], which makes it difficult to predict the energy barrier from the LUMO energy values of the single materials. In general, our model does not include such an energy barrier and so far we find that it is not needed to consider it.

3. Modeling the electrothermal feedback

After we have modeled all experimental data, we will now use our global fit parameters to understand electrothermal feedback in OLEDs in more detail. Figure 1 already presented the experimental data for a pulsed measurement which shows no self-heating and a curve measured in the steady state, which shows a pronounced voltage turnover and a regime of NDR.

To account for electrothermal feedback, we use the derived explicit expressions to describe the current flow at each voltage and temperature, and introduce a coupling to the dissipated energy

$$\Delta T = \Theta_{\text{th}} P_{\text{el}}, \qquad (5)$$

which will in turn lead to a temperature increase ΔT of the device. Here, Θ_{th} is the thermal resistance and P_{el} is the electrically generated power. The fact that the outcoupled light will not lead to device heating is omitted here and primarily incorporated into the fitting of the thermal resistance which will consequently differ by the power plug efficiency of the OLED being around 10%.

First, the thermal resistance is set to 0 and the model reproduces the pulsed measurement which is assumed to be isothermal over the entire range. However, merely by changing the thermal resistance to 185 K/W, the steady-state current-voltage curve is reproduced, including the regime where a strong electrothermal feedback takes place. Thus, our model can recover the device operation over nine orders of magnitude, including recombination, drift limitation, and nonlinear electrothermal feedback.

As already mentioned above, the fit has to be understood to be a global fit matching all three data sets of Figs. 1, 3, and 4. To achieve this we accepted to have some disagreement between the model and experiment at very low voltages, but mainly concentrated on matching data from room temperature to higher temperatures as this is the range where self-heating takes place. Furthermore, it is known that electrothermal feedback leads to inhomogeneous current flow and light emission inside the active area. Still, the zero-dimensional model approach works quite well, simply because the active area is rather small so that the inhomogeneity is less pronounced and the presented current densities as well as the fitted thermal resistance have to be understood as mean values.

B. Further evaluation of the model

The model now enables us to perform some further evaluation. First, we can calculate the mean temperature
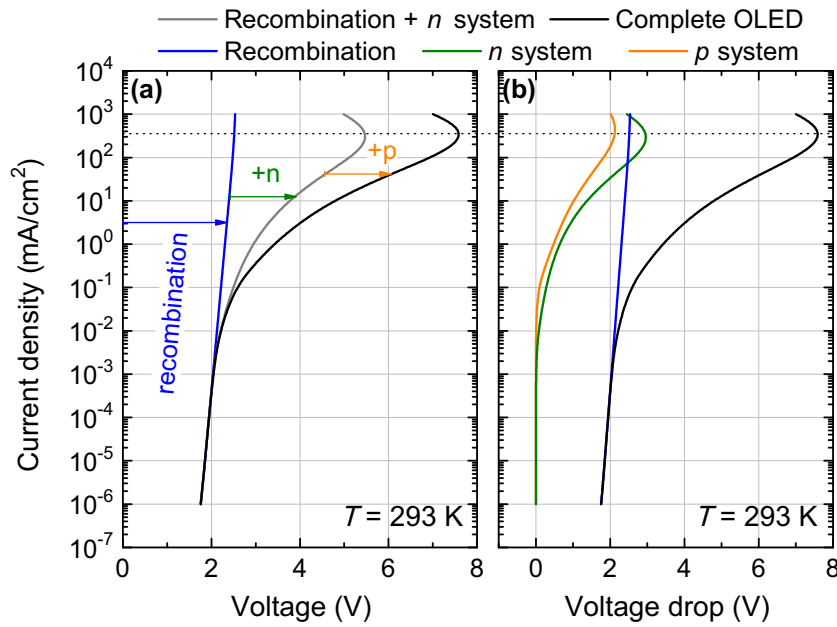
FIG. 5.   Modeled curves corresponding to the fit in Fig. 1 including electrothermal feedback. (a) Cumulative voltage drop for the sequence recombination, the *n* system (+*n*) and the *p* system (+*p*). The *n* system consumes most of the applied potential at high current densities, whereas at low current densities the OLED is fully determined by recombination in the exponential current-voltage regime. (b) The individual voltage drops for each system. The dashed horizontal line represents the voltage turnover of the complete OLED. It can be seen that the voltage turnover of the *n* system happens at lower current densities whereas the *p* system has a voltage turnover at higher current densities. Thus, electrothermal feedback in OLEDs can internally affect the layers differently.

increase of the sample due to self-heating by using Eq. (5). As indicated in Fig. 1, shortly before degradation occurs an increase by 83.6 K results in a mean device temperature of 376.6 K. Measurements using external heating show that samples start to degrade in the range between 360 and 385 K in accordance with the simulated value (see Fig. S3 in the Supplementary Material [13]). The mean temperature increase at the turnover point is about 33 K, and thus sufficiently low to prevent degradation at this point.

Besides that, the model reveals the voltage distribution between the *n* system, the recombination, and the *p* system for each current density as shown in Fig. 5. Up to current densities of 10^{-2} mA/cm^2, the current-voltage characteristics are exponential and the filling of the states and their recombination dominates. Then, the voltage drop of the *p* and the *n* system increases and, e.g., at 10 mA/cm^2, both systems together consume more of the applied voltage than the recombination. Whenever these drift components limit the current flow in an OLED, it is likely that the charge carrier balance is influenced and most likely the region where electrons and holes meet shifts towards the system with the lowest conductivity, which is the *n* system in our case. It is already known from the literature that a very similar layer stack has a recombination zone located at the hole-blocking layer (Balq2) [16]. This charge-carrier imbalance does not have to change the current efficiency of the OLED as all of the injected charge carriers could still have the same probability to recombine radiatively. However, the increasing voltage consumption definitely changes how the applied voltage is effectively used and thus the "voltage efficiency". For example, the emitted light remains to have the same energy of ca. 2 eV, even if, e.g., 5 V is applied

to the OLED. As a consequence, the power efficiency always drops whenever the voltage at the *n* or the *p* system becomes significantly large.

For the highest current densities in Fig. 5, we discuss the effect of each system onto the electrothermal feedback. The horizontal black dashed lines represent the current density at which the voltage turnover of the complete OLED takes place. It can be seen that the recombination does not show any strong voltage reduction and thus does not contribute significantly to the voltage turnover. Contrary to that, the *p* and *n* systems show a pronounced electrothermal feedback at current densities around 400 mA/cm^2, which is the main reason why we see electrothermal feedback in a complete OLED. We further find that the turnover of the *n* system takes place slightly below the level at which it happens for the OLED while the *p* system has the turnover slightly above this level. This behavior can be explained by the higher activation energies for the electrical conductivity of the *n* system with respect to the *p* system in accordance with Fig. 3. To further answer the question of which part of the OLED has the most influence, we can use Fig. 4(b) in which the activation energy is derived from the model. In the voltage range, where self-heating occurs, i.e., above 5 V, the activation energy is mostly influenced by the *p* and the *n* system, leading to a saturation around 0.3 eV, which is in between the activation energies we found for each individual system in Fig. 3 at larger voltages (>1 V). The activation of the electrical conductivity arising from the recombination, however, is smaller. At the current density at which the turnover takes place, 2.51 V is needed for the recombination. The recombination current itself has a remaining activation energy of 0.136 eV, as given by Eq. (2). This value is sufficiently high to allow for

electrothermal feedback as ∼0.1 eV ($4k_BT$) is typically needed at room temperature [11]. However, the smaller the activation energy, the higher the temperature rise has to be to achieve the voltage turnover, so that in this case the recombination current does not reach this point.

C. Origin of the activation energy

With the knowledge that the electrothermal feedback mainly arises from potential drops in the electron- and hole-conducting system, we can use in-depth studies of single-carrier devices to elaborate which mechanism contributes most to the temperature-activated conductivity. In Fig. 6, the current-voltage curves of fully-n-doped and fully-p-doped devices of various thicknesses without an intrinsic layer are shown as well as n-i-n and p-i-p devices with a constant doped layer thickness (30 nm). Devices with no intrinsic layer display almost no thickness dependence at low voltages, which points to the fact that charge transport through the doped layer is very efficient. This fact is often used when the cavity length of an OLED is adjusted to the first or second optical maximum without changing the electrical properties much [39]. Only the curve of the thinnest sample for the n system differs. It should be noted that these devices can be reproducibly compared, as they are produced within one fabrication run and they even partially share the same layers as the different thicknesses are achieved by a moving shutter. At higher voltages, it is interesting to see that these curves become nonlinear and deviate from each other in a way that the current is higher, the thinner the sample is. This behavior is in accordance with space-charge-limited currents which have a pronounced thickness dependence ($\propto L^{-3}$) and typically are clearly visible at voltages above 1 V. The fact that these devices show no thickness dependence at low

voltages indicates that they are limited by a common property, which is most likely caused by the interfaces to the metal electrodes. These interfaces remain the same, independent of thickness. Thus, it is likely that even though the layers are doped, intentionally done to reduce the contact resistance, they still exhibit a significant contact resistance for charge injection which is at least much higher than the bulk resistance of the thickest device. Doping technology is nowadays successfully used in organic light-emitting diodes to improve charge injection but it still seems that there is room for further improvement [43,44].

If we now insert an intrinsic layer exactly into the middle of a doped device, we can study the influence of the intrinsic layer as well as the influence of the possible energy barrier at the organic-organic interface between the doped and the intrinsic layer. As shown in Figs. 2(a) and 2(c), these devices then have 30-nm-doped layers surrounding the intrinsic layer. For the p system, inserting up to 30 nm of intrinsic material does not drastically change the current flow. The reduction of the current can simply be explained by the fact that a more resistive part is introduced into the device which has a lower charge-carrier concentration. Furthermore, at higher voltages, where we expect to reach space-charge-limited current, the thickness dependence is less pronounced and can partially be attributed to the fact that a device with a 30-nm intrinsic layer is 50% thicker than a device without an intrinsic layer, and thus the thickness-dependent SCLC is expected to drop already by a factor of about 3. In the complete OLED, a 10-nm intrinsic p-type layer is used which does not make a big difference in Fig. 6. Therefore, an internal energy barrier as well as a larger resistive contribution of the intrinsic layer can be disregarded. It merely seems that the temperature-activated conductivity in Fig. 3 arises from an injection
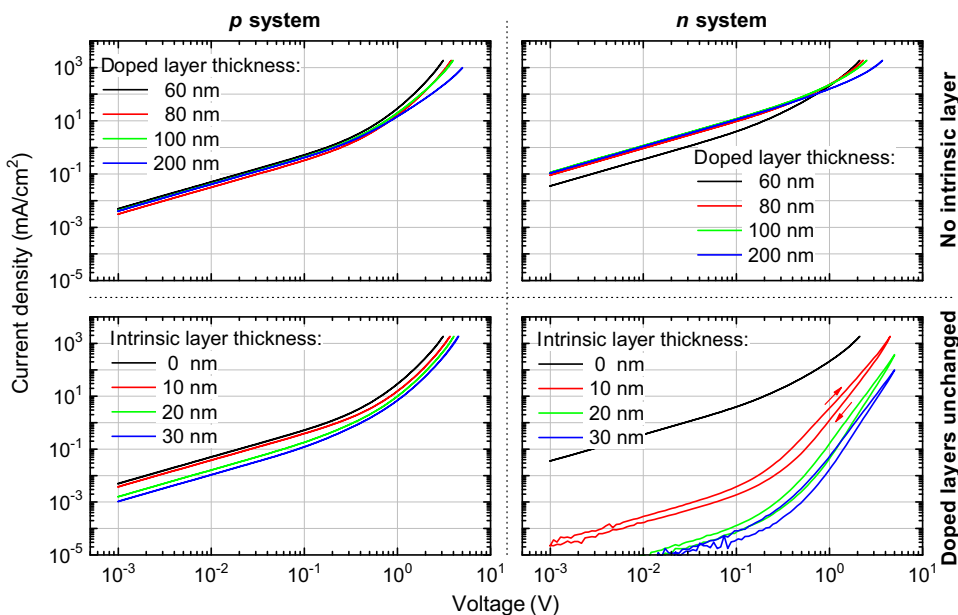

FIG. 6. Experimental current-voltage curves of p-i-p (left) and n-i-n (right) devices. The upper two graphs show samples without an intrinsic layer and a variation of the total doped layer thickness. The lower two graphs show samples with a 30-nm-doped layer below and above the intrinsic layer. While the p system is less affected by inserting an intrinsic layer, the n system shows a strong reduction of conductivity upon introducing even just 10 nm of intrinsic material.

resistance at low voltages and a general charge-transport limitation at higher voltages.

The situation is rather different for the *n* system. Introducing an intrinsic layer in the middle of a doped device strongly changes the sample conductivity [see Fig. 2(c)]. Even 10 nm of intrinsic material changes the current already by three orders of magnitude at the lowest voltages in the linear regime. At higher voltage in the superlinear regime, the curves for different thicknesses approach each other, but still differ significantly. Thus, a simple layer thickness dependence due to SCLC can be excluded. In the case of the *n* system, it is more likely that the intrinsic layer introduces an energy barrier for electrons as visualized by an arrow in Fig. 2(f). An alternative explanation would be to consider trap states in the intrinsic layer which can explain the clockwise hysteresis after insertion of the intrinsic layer. However, the trap-state density must be extremely large if a 10-nm layer is able to decrease the sample conductivity by three orders of magnitude. For that reason, we still tend to expect a main impact from an energy barrier.

Then, charge carriers will accumulate in front of the interface between the doped and the intrinsic layer in order to increase the electric field in the intrinsic layer. When higher voltages (>1 V) are applied, the electric field can get sufficiently high so that charge carriers overcome the internal energy barrier and the influence of the intrinsic layer onto the current-voltage characteristics decreases as seen in Fig. 6. The temperature-activated conductivity of the *n* system is thus much more related to the intrinsic layer. At the lowest voltage, the intrinsic layer introduces a region of much lower charge-carrier concentration due to the missing doping and the higher energy level which comes along with the internal energy barrier. The activation energy of the electrical conductivity, estimated to be 0.5 eV, is thus directly related to this internal energy barrier and it can be assumed that the energy difference of the transport levels between the doped and the intrinsic level is on the order of the activation energy. At higher voltages, the internal energy barrier can be overcome more easily and the estimated activation energies also decrease to about 0.325 eV [cf. Fig. 3(d)].

To realize OLEDs with reduced electrothermal feedback, very low activation energies of the electrical conductivity are necessary and they can be achieved by optimizing the layer-stack design. First, the internal energy barriers have to be avoided as they not only decrease the performance of an OLED, but also introduce high activation energies to the system. Furthermore, doped layers, typically believed to solve issues with contact resistance, do still underperform and do not allow the highest possible currents which would be possible for these materials. If these issues can be solved, the voltage losses at the *p* and *n* systems decrease so that their activation energies do affect the current-voltage-temperature curves to a

lesser extent. However, the lowest-activation energies will always be given by the charge transport, typically in the range of 100 to 200 meV depending on the width of the Gaussian density of states [11]. Only in the case of a negligible drift limitation, the activation energy of the electrical conductivity could be lower. As the activation energy of the recombination current decreases with voltage, it could theoretically approach zero for $V = E_{a,0}/e$ (see Fig. 4).

III. CONCLUSION

We introduce a full electrothermal model for OLEDs applicable over a wide range of current densities and application-relevant temperatures. Our approach is, in principle, adaptable to any semiconductor diode, e.g., an organic solar cell where recombination as well as conduction of charges takes place. The explicit description can be used to predict the behavior of an OLED in real electronic circuits as it is already implemented using circuit models and our parametrization is ideal for further use in spatially resolved multidimensional simulations [45]. Furthermore, due to the description of the activation energies of the electrical conductivities of the OLED, the model fully accounts for strong nonlinear electrothermal feedback and self-heating effects. Such a description will also support the first realization of an electrically pumped organic laser where strong pumping will lead to self-heating too [46,47].

The model predicts which regions have the highest electrical potential drop and therefore contribute most to the overall activation energy of the electrical conductivity of the OLED. By that, internal energy barriers can be identified to be the most influential factor. Finally, as a side product, we give here a temperature- and voltage-dependent description of the recombination current in OLEDs which has not been reported so far and can become an essential tool to study OLEDs. Overall, our model gives a comprehensive analysis of the operation of an OLED from the electrothermal point of view and thus will help scientists working on emerging thin-film LED technologies to extract the most out of their current-voltage characteristics as well as helping engineers to optimize OLEDs for high-brightness applications, e.g., as found in the automobile sector.

[1] Ruiqing Ma, in *Handbook of Visual Display Technology*, edited by Janglin Chen, Wayne Cranton, and Mark Fihn (Springer International Publishing, Cham, 2016), p. 1821.

[2] Yonghee Cho and Tugrul Daim, OLED TV technology forecasting using technology mining and the Fisher-Pry diffusion model, Foresight **18,** 117 (2016).

[3] Yifan Zhang, Jaesang Lee, and Stephen R. Forrest, Tenfold increase in the lifetime of blue phosphorescent organic light-emitting diodes, Nat. Commun. **5,** 5008 (2014).

[4] Kevin J. Bergemann, Robert Krasny, and Stephen R. Forrest, Thermal properties of organic light-emitting diodes, Org. Electron. **13,** 1565 (2012).

[5] Philipp Schwamb, Thilo C. G. Reusch, and Christoph J. Brabec, Passive cooling of large-area organic light-emitting diodes, Org. Electron. **14,** 1939 (2013).

[6] M. Slawinski, D. Bertram, M. Heuken, H. Kalisch, and A. Vescan, Electrothermal characterization of large-area organic light-emitting diodes employing finite-element simulation, Org. Electron. **12,** 1399 (2011).

[7] Axel Fischer, Thomas Koprucki, Klaus Gärtner, Max L. Tietze, Jacqueline Brückner, Björn Lüssem, Karl Leo, Annegret Glitzky, and Reinhard Scholz, Feel the heat: Nonlinear electrothermal feedback in organic LEDs, Adv. Funct. Mater. **24,** 3367 (2014).

[8] Heinz Bässler and Anna Köhler, in *Unimolecular and Supramolecular Electronics I*, Topics in Current Chemistry, Vol. 312, edited by Robert M. Metzger (Springer, Berlin, Heidelberg, 2012) p. 1.

[9] L. Pohl, E. Kollár, A. Poppe, and Z. Kohári, Nonlinear electro-thermal modeling and field-simulation of OLEDs for lighting applications I: Algorithmic fundamentals, Microelectronics J. **43,** 624 (2012).

[10] Jan Buytaert, Johan Bleumers, Alexander Steen, and Peter Hanselaer, Optical determination of the junction temperature of OLEDs, Org. Electron. **14,** 2770 (2013).

[11] Axel Fischer, Paul Pahner, Björn Lüssem, Karl Leo, Reinhard Scholz, Thomas Koprucki, Klaus Gärtner, and Annegret Glitzky, Self-heating, Bistability, and Thermal Switching in Organic Semiconductors, Phys. Rev. Lett. **110,** 126601 (2013).

[12] Matthias Liero, Thomas Koprucki, Axel Fischer, Reinhard Scholz, and Annegret Glitzky, *p*-Laplace thermistor modeling of electrothermal feedback inorganic semiconductor devices, Zeitschrift für angewandte Mathematik und Physik **66,** 1 (2015).

[13] See Supplemental Material at https://link.aps.org/supplemental/10.1103/PhysRevApplied.10.014023 for further experimental data supporting our findings.

[14] Toshinori Matsushima and Chihaya Adachi, Observation of extremely high current densities on order of MA/cm^2 in copper phthalocyanine thin-film devices with submicron active areas, Jpn. J. Appl. Phys. **46,** L1179 (2007).

[15] T. P. I. Saragi, T. Fuhrmann-Lieker, and J. Salbeck, Comparison of charge-carrier transport in thin films of Spiro-linked compounds and their corresponding parent compounds, Adv. Funct. Mater. **16,** 966 (2006).

[16] Rico Meerheim, Sebastian Scholz, Selina Olthof, Gregor Schwartz, Sebastian Reineke, Karsten Walzer, and Karl Leo, Influence of charge balance and exciton distribution on efficiency and lifetime of phosphorescent organic light-emitting devices, J. Appl. Phys. **104,** 014510 (2008).

[17] Axel Fischer and Felix Kaschura, *SweepMe! - a multi-tool measurement software (sweep-me.net)*, Dresden, Germany (2016).

[18] Axel Fischer, Paul Pahner, Björn Lüssem, Karl Leo, Reinhard Scholz, Thomas Koprucki, Jürgen Fuhrmann, Klaus Gärtner, and Annegret Glitzky, Self-heating effects in organic semiconductor crossbar structures with small active area, Org. Electron. **13,** 2461 (2012).

[19] G. A. H. Wetzelaer, M. Kuik, H. T. Nicolai, and P. W. M. Blom, Trap-assisted and Langevin-type recombination in organic light-emitting diodes, Phys. Rev. B **83,** 165204 (2011).

[20] Peter Mark and Wolfgang Helfrich, Space-charge-limited currents in organic crystals, J. Appl. Phys. **33,** 205 (1962).

[21] P. N. Murgatroyd, Theory of space-charge-limited current enhanced by Frenkel effect, J. Phys. D: Appl. Phys. **3,** 151 (1970).

[22] G. A. H. Wetzelaer and Paul W. M. Blom, Diffusion-driven currents in organic-semiconductor diodes, NPG Asia Mater. **6,** e110 (2014).

[23] Jason A. Röhr, Thomas Kirchartz, and Jenny Nelson, On the correct interpretation of the low voltage regime in intrinsic single-carrier devices, J. Phys. Condens. Matter **29,** 205901 (2017).

[24] J. Campbell Scott, Metal-organic interface and charge injection in organic electronic devices, J. Vac. Sci. Technol. A: Vac. Surfaces Films **21,** 521 (2003).

[25] R. Coehoorn, W. F. Pasveer, P. A. Bobbert, and M. A. J. Michels, Charge-carrier concentration dependence of the hopping mobility in organic materials with Gaussian disorder, Phys. Rev. B: Condens. Matter Mater. Phys. **72,** 155206 (2005).

[26] N. I. Craciun, J. Wildeman, and P. W. M. Blom, Universal Arrhenius Temperature Activated Charge Transport in Diodes from Disordered Organic Semiconductors, Phys. Rev. Lett. **100,** 056601 (2008).

[27] M. Schober, M. Anderson, M. Thomschke, J. Widmer, M. Furno, R. Scholz, B. Lüssem, and K. Leo, Quantitative description of charge-carrier transport in a white organic light-emitting diode, Phys. Rev. B: Condens. Matter Mater. Phys. **84,** 165326 (2011).

[28] E. F. Schubert, *Light-Emitting Diodes* (Cambridge University Press, New York, 2006).

[29] M. Kuik, L. J. A. Koster, G. A. H. Wetzelaer, and P. W. M. Blom, Trap-assisted Recombination in Disordered Organic Semiconductors, Phys. Rev. Lett. **107,** 256805 (2011).

[30] S. M. Sze and Kwok K. Ng, *Physics of Semiconductor Devices*, 3rd ed. (John Wiley and Sons, New York, 2007).

[31] L. J. A. Koster, V. D. Mihailetchi, R. Ramaker, and P. W. M. Blom, Light intensity dependence of open-circuit voltage of polymer: fullerene solar cells, Appl. Phys. Lett. **86,** 123509 (2005).

[32] Martijn Kuik, Herman T. Nicolai, Martijn Lenes, Gert-Jan A. H. Wetzelaer, Mingtao Lu, and Paul W. M. Blom,

Determination of the trap-assisted recombination strength in polymer light emitting diodes, Appl. Phys. Lett. **98,** 093301 (2011).

[33] Kristofer Tvingstedt and Carsten Deibel, Temperature dependence of ideality factors in organic solar cells and the relation to radiative efficiency, Adv. Energy Mater. **6,** 1502230 (2016).

[34] C. Sah, R. N. Noyce, and W. Shockley, Carrier generation and recombination in p-n junctions and p-n junction characteristics, Proc. IRE **45,** 1228 (1957).

[35] Uli Würfel, Dieter Neher, Annika Spies, and Steve Albrecht, Impact of charge transporton current–voltage characteristics and power-conversion efficiency of organic solar cells, Nat. Commun. **6,** 6951 (2015).

[36] Marc Dvorak, Su-Huai Wei, and Zhigang Wu, Origin of the Variation of Exciton Binding Energy in Semiconductors, Phys. Rev. Lett. **110,** 016402 (2013).

[37] Kuo-Chun Tang, Kuan Lin Liu, and I-Chia Chen, Rapid intersystem crossing in highly phosphorescent iridium complexes, Chem. Phys. Lett. **386,** 437 (2004).

[38] Dong Zhao, Hans-Peter Loebl, and Volker Van Elsbergen, Transient luminescence in organic light-emitting diodes explained by trap-assisted recombination of stored charges, Org. Electron. **14,** 3117 (2013).

[39] Caroline Murawski, Philipp Liehm, Karl Leo, and Malte C. Gather, Influence of cavity thickness and emitter orientation on the efficiency roll-off of phosphorescent organic light-emitting diodes, Adv. Funct. Mater. **24,** 1117 (2014).

[40] A. Köhler and H. Bässler, Tripletstates in organic semiconductors, Mater. Sci. Eng.: R: Reports **66,** 71 (2009).

[41] Wolfgang Brütting, Stefan Berleb, and Anton G. Mückl, Device physics of organic light-emitting diodes based on molecular materials, Org. Electron. **2,** 1 (2001).

[42] Simon Züfle, Stéphane Altazin, Alexander Hofmann, Lars Jäger, Martin T. Neukom, Tobias D. Schmidt, Wolfgang Brütting, and Beat Ruhstaller, The use of charge extraction by linearly increasing voltage in polar organic light-emitting diodes, J. Appl. Phys. **121,** 175501 (2017).

[43] Jingsong Huang, Martin Pfeiffer, Ansgar Werner, Jan Blochwitz, Karl Leo, and Shiyong Liu, Low-voltage organic electroluminescent devices using pin structures, Appl. Phys. Lett. **80,** 139 (2002).

[44] Martin Oehzelt, Norbert Koch, and Georg Heimel, Organic semiconductor density of states controls the energy level alignment at electrode interfaces, Nat. Commun. **5,** 4174 (2014).

[45] Matthias Liero, Jürgen Fuhrmann, Annegret Glitzky, Thomas Koprucki, Axel Fischer, and Sebastian Reineke, 3D electrothermal simulations of organic LEDs showing negative differential resistance, Opt. Quant. Electron. **49,** 330 (2017).

[46] Kou Yoshida, Toshinori Matsushima, Hajime Nakanotani, and Chihaya Adachi, Quantification of temperature rise in unipolar organic conductors during short voltage-pulse excitation using electrical testing methods, Org. Electron. **31,** 191 (2016).

[47] Irma Slowik, Axel Fischer, Hartmut Fröb, Simone Lenk, Sebastian Reineke, and Karl Leo, Novel organic light-emitting diode design for future lasing applications, Org. Electron. **48,** 132 (2017).